Development of 90 GHz microwave radiometer sensor in snow/ice studies over the Himalaya as input for disaster monitoring

Vasudha, M. P.*, G. Raju and N. Thangadurai

Department of Electronics and Communication Engineering, School of Engineering and Technology, Jain (Deemed-to-be University), Bengaluru 562 112, India

In this study, a sensor is designed based on a basic radiometer system at 18.8 GHz for ground-based testing and operations. Initially a generic radiometer will be designed in total power radiometer configuration (Phase 1) that is more appropriate for remote sensing platforms for operations in a campaign mode, such as an airborne mission. The same radiometer is proposed to be modified as a null-balancing Dicke radiometer (Phase 2) that is more suitable for long-term field operations over a range of temperatures and environmental conditions. This system is also useful for long-term propagation experiments in communication. The development of a millimeter-wave radiometer is in several hardware realization phases identified as Phases 1 and 2. The present proposal is expected to facilitate realization and utilization of microwave radiometers for space applications. The team at Jain University, Bengaluru will complement activities at ISRO in remote sensing applications through any campaigns proposed by the latter. Any future incremental development activities such as augmentation at higher frequencies as well testing newer concepts such as phased-array antenna for electronic scanning at lower frequencies, dichroic antennas at very high frequencies, etc. may be attempted based on the trends in technology/hardware.

Keywords: Disaster monitoring, microwave radiometer, remote sensing, snow/ice studies.

THE wide range of natural/man-made calamities of the Indian subcontinent include rapid reduction in volume of Himalayan glaciers, loss of freshwater, cyclones, floods, droughts, earthquakes, etc. The causes of such calamities are global warming, perturbation in thermal structure of the ocean, variation in rainfall, variation in the behaviour of the Earth's atmosphere, etc.[1]. Consequences of these calamities are: climatic variability, biodiversity and damage to the ecosystems. Efficient control and/or prevention of such calamities must be done by monitoring the disasters caused by them.

The geological regions to be monitored are: the Himalaya, including the Tibetan region and oceans around the Indian subcontinent, viz. the Bay of Bengal, Arabian Sea and Indian Ocean[8,9]. The Himalaya is the world's third largest region of glaciers covering approximately 2400 km, and passing through India (NE), Pakistan[6,15], Afghanistan[16], China[20], Bhutan[17] and Nepal[19]. It consists of the Siachen and the Biafo glaciers measuring about 60–70 km, and 46 other notable glaciers in four different states of India[10,11,21]. Himalayan glaciers feed major South Asian rivers like the Indus, the Brahmaputra and the Ganges. Since 1970s, there has been serious decrease in accumulation and/or mass balance that drastically increases ablation of the glaciers. The major hazards caused by melting Himalayan glaciers are catastrophic events like floods, dangerous sea conditions, etc. Due to inaccuracy in ground-based observations and paucity of consistent and reliable data, airborne observations are necessary[12–14].

Microwave radiometers find applications in weather forecasting and climate change studies. Advanced radiometer techniques and applications are continuously evolving and realized in new space missions. Measurement of sea surface winds is one of the important parameters in these applications, and microwave radiometers can acquire data during all-weather conditions with good accuracy. Physical parameters to be measured/monitored include: sea surface winds, accumulation, extent of accumulation and ablation of glaciers, ice/snow, rainfall estimates, atmospheric humidity and sea-surface temperature (SST)[15].

Due to paucity in *in-situ* measurements of sea surface winds, which are normally derived from instruments on shorelines, ships, buoys and global measurements, data were obtained from satellite observations. It is difficult to obtain data in all-season and all-environmental conditional measurements. Hence, there is need for measurement of near ocean surface from airborne or ground (tower-mounted) missions. Therefore, the aim of this study is to develop a radiometer system for ground-based applications followed by airborne operations and adoptable for satellite missions.

Scientific, technical and/or techno-economic importance of the present study is as follows.

(a) To develop a ground-based microwave radiometer followed by laboratory and field tests conducted to

*For correspondence. (e-mail: vasudhamysore2019@gmail.com)

Table 1. Examples of Earth observing satellite missions (ocean/sea surface wind measurement) which provide valuable information

Satellite	Launched date and orbit	Agency	Instrument	Scanning technique	Coverage/cycle
Terra (EOS AM-1)	16 December 1999 till now; sun synchronous.	NASA, USA	Moderate Resolution Imaging Spectro-Radiometer (MODIS)	Whiskbroom scanning Swath: 2230 km Data rate: 6.2 Mbps	Global coverage twice/day
Aqua	4 May 2002 till now' sun synchronous.	NASA, USA	Moderate Resolution Imaging Spectro-Radiometer (MODIS)	Whiskbroom scanning Swath: 2230 km Data rate: 6.2 Mbps	Global coverage twice/day
Coriolis	6 January 2003 till now; sun synchronous.	DoD, NASA, USA	WindSat	Conical: 50–55° zenith angle. Swath: 1000 km Antenna dia: 1.83 m Data rate: 35 kbps	Global in 1.5 days
NOAA-19	6 February 2009 till now; sun synchronous.	NOAA, USA	Advanced Very High Resolution Radiometer/3 (AVHRR/3)	Swath: 2900 km Data rate: 621.3 kbps. Freq band: visible near IR, thermal IR.	Global coverage twice/day
GCOM-W1	January 2012 till now; sun synchronous.	JAXA, Japan	Advance Microwave Scanning Radiometer-2 (AMSR-2)	Conical: 55° zenith angle. Swath: 1450 km Antenna dia: 2 m Data rate: 130 kbps	Global coverage once/day
HY-2A/Ocean-2A	15 August 2011 till now; near sun synchronous frozen orbit.	NSOAS, China	Microwave Radiometer Imager (MWRI)	Conical: 55° zenith angle. Swath: 1600 km Antenna dia: 1.2 m	Daily global coverage

determine the primary sensor performance, such as sensitivity, stability, calibration and repeatability.

(b) The radiometer system to be developed can be operated initially from a stationary tower and subsequently from an airborne platform.

(c) The radiometer system can be used both for field performance and concurrent observations in a campaign mode for satellite sensor validation.

(d) To obtain data from inaccessible regions with accuracy, equivalent to microwave sensors used in current Earth observation satellite missions.

(e) Multiple units of the final qualified version can be designed and used for more widespread experiments based on scientific applications.

(f) Similar radiometers with minimal but essential changes (especially the centre frequency) may be used and adapted for a large number of applications such as: (i) SST studies in the C-band. (ii) Soil moisture/ocean salinity in the L-band. (iii) Snow/ice studies at frequencies 36 GHz and up to 157 GHz based on funding. (iv) Atmospheric sounders to measure temperature and humidity at 60/183 GHz. (v) Medical diagnostics applications in L-band.

(g) There are promising possibilities for academic institutions and user agencies for expanding the research and applications, once the basic system is realized satisfactorily.

(h) External collaboration is also a good possibility for scientific/technical enrichment.

(i) The system can also be considered (after optimization) for production by industry, either partly or wholly.

(j) The system when fully validated can be easily commercialized since the demand will grow when applications are demonstrated.

This study proposes to secure the most consistent and reliable data from remote sensing method using airborne 90 GHz millimetre-wave radiometer with special reference to glaciers in the Himalaya.

Background

Currently, the traditional field-based, *in situ* glaciological monitoring, supplemented by remote sensing techniques is sparse and lacks consistency. Both categories of data are obtained from global Earth observation satellites (equipped with remote sensing instruments) and glaciological monitoring. The data from monitoring glacier precipitation and glacier melting are used for monitoring hazards caused by such events. This procedure again suffers from serious lack of reliable and consistent data. Therefore it is important that more missions are conducted for the purpose of disaster monitoring, particularly for monitoring the Himalayan glacier regions. Considering the Himalayan regions, it is envisaged that two constellations of small satellites equipped with appropriate sensors with fine or high-resolution potential be used for effectively conducting regional and global surveys complemented by airborne and ground-based observations.

Past spaceborne missions as well as those currently under operation have been equipped with effective

microwave remote-sensing instruments that have proven their capability to predict, monitor and track cyclones, extent of glaciers or ice snow properties[7]. The spaceborne missions operating at present are: US-JAXA Tropical Rain Mapping Mission (TRMM), Aqua, Windsat, SeaWinds, QuikScat, ENVISAT and the Indian satellites OCEANSAT-2 and Megha-Tropiques. Table 1 lists several missions highlighting the current global scenario.

Methodology

To measure and/or monitor disaster caused by ablation of glaciers in the Himalaya, it is proposed to launch a small satellite to form one of the constellation satellites in an inclined orbit. A small satellite is launched in an inclined orbit similar to TRMM. This satellite will make about 2–4 observations per day from 800 km orbit. This proposal envisages a complex active–passive sensor: a 90 GHz radiometer and an L-band synthetic-aperture radar (SAR) combination to detect and monitor ice/snow melting in the Himalayan regions[4,5].

The total power microwave radiometer is utilized to acquire information from radiation emitted or reflected by natural Earth objects by ground-based operation (or near *in situ* observations). It functions under all weather conditions, except rainfall with the same accuracy as IR sensors. A microwave radiometer has several advantages over other types of receivers. Some of these have high sensitivity, high stability, high accuracy and good signal-to-noise ratio.

A radiometer using the technique of heterodyne for measuring microwaves was first reported in 1946 (refs 3, 12). This technique is used for spectral decomposition of radiation received by the radiometer. The principle of heterodyne detection involves three distinct processes. First, the radiofrequency (RF) signal which is received by the radiometer is mixed with the signal from a local oscillator. In this stage the frequency spectrum of the original signal is translated to a much lower frequency named as intermediate frequency (IF); Figure 1. The resulting IF signal is subsequently amplified, and finally detected and processed in a video circuit. In the process of frequency down-conversion, three essential components are identified. These are local oscillator, mixer and an intermediate frequency output port.

We propose a total power radiometer as its sensitivity is almost two times better than the Dicke radiometer. At 18 GHz, it is possible to develop and/or procure stable front-end subsystems of the radiometer. As an extension of this, a 'noise-injection/null-balancing' radiometer is also planned to be developed as Phase 2 activities (Figure 2).

The development is implemented in the following stages: (a) Feasibility study, (b) System design, (c) Subsystem design: partly developed and partly procured, (d) The major subsystems include: (i) RF units – antenna, feed and support structure (scan mechanism in Phase 3 only). Highly stable front-end amplifier/low-noise amplifier/ direct detection amplifier. (ii) Back-end – Detector, DC amplifier, and ADC and storage system. (e) System integration and laboratory calibration. (f) Field operations and validation. (g) Airborne operations (Phase 3 only).

General specifications of the ground-based/airborne radiometer are as follows:

- Nominal altitude: 3–8 km (above ground-level to be worked out after discussions with aircraft operators).
- Total payload power required: 10–15 W.
- Antenna diameter: 30–40 cm.
- Antenna: dual linear polarization (*V* and *H*); horn feed; offset parabolic reflector.
- Mechanically scanning antenna.
- Spatial resolution: <20–40 m.
- Sensitivity: less than 0.4 K.
- Scan angle: 30°–45°.
- Swath: 4–10 km (depending on height of flight, scan angle and antenna diameter).
- Noise figure (NF): less than 2 dB.

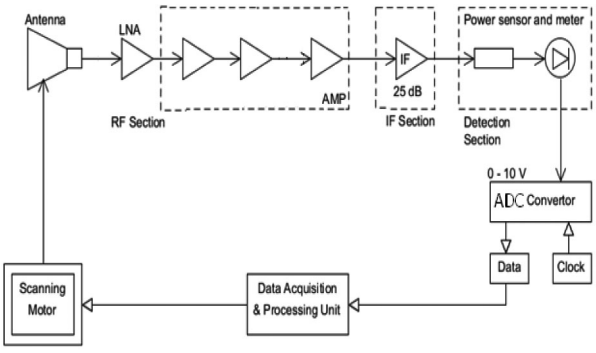

Figure 1. Mechanical scanning microwave radiometer preliminary block diagram.

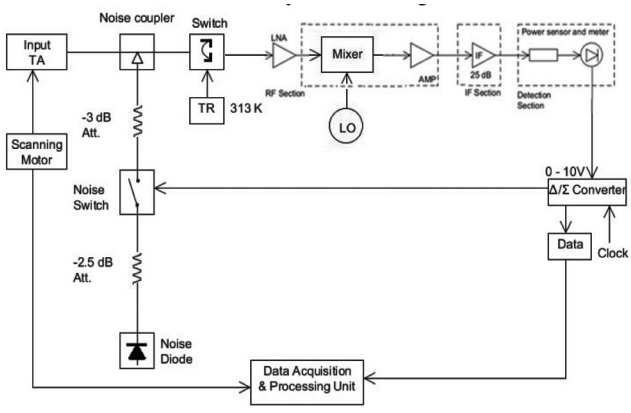

Figure 2. Noise injection microwave radiometer preliminary block diagram[12].

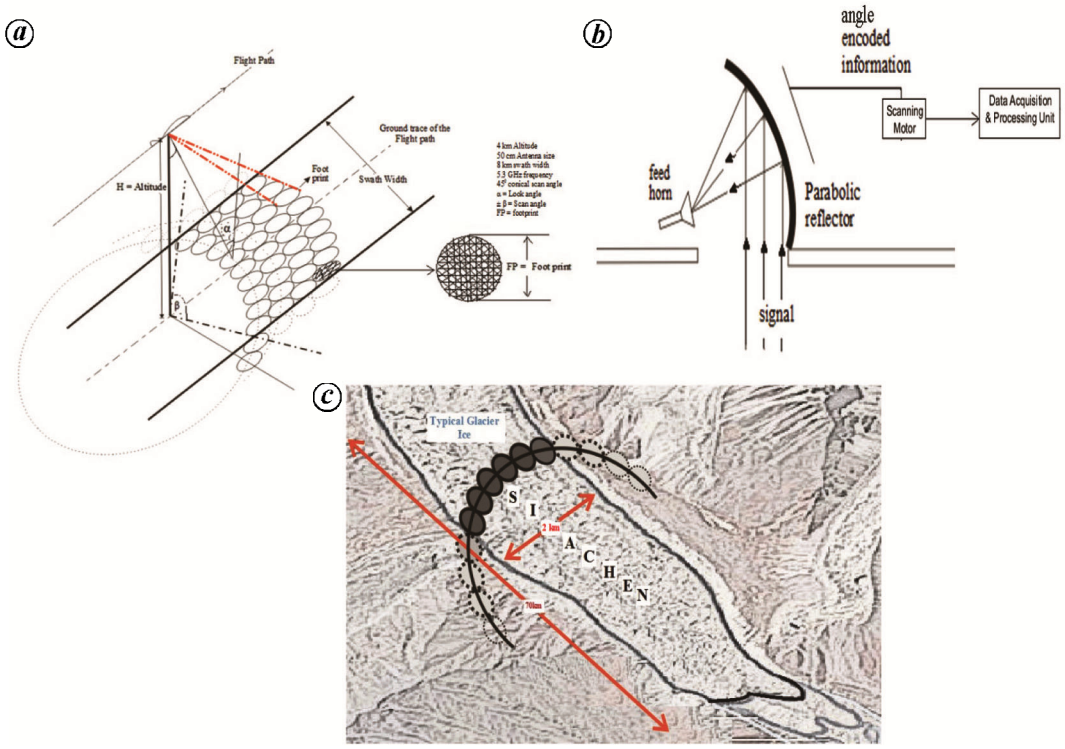

Figure 3. ***a***, Conical scanning mechanism. ***b***, Mounting system of antenna. ***c***, Siachen glacier scanning.

Table 2. Beam-width (ψ) and footprint (FP_N)

	ψ	FP_N for 360°	FP_N for 90°
f = 5.3 GHz, λ = 0.0566 m	7.9°~8°	45	11.25~12
f = 6.0 GHz, λ = 0.05 m	7°	51.43~52	12.85~13
f = 6.9 GHz, λ = 0.0434 m	6.09°~6.1°	59.01~59	14.75~15
f = 11 GHz, λ = 0.0272 m	3.82°	94.24~94	23.56~24
f = 18.8 GHz, λ = 0.016 m	2.24°	160.71~161	40.17~40

Figure 3 *a* shows the conical scanning mechanism along with footprint size calculation, while Figure 3 *b* and *c* shows antenna mounting and scanning over Siachen glacier. Table 2 shows the relationship between beam width (ψ) and the number of footprints (FP_N) where $\psi = 70 \times (\lambda/D)$ degrees; D is the diameter of the antenna = 0.5 m = 50 cm; and $FP_N = (360°/\psi)$.

Table 3 shows the relationship between altitude (H) and footprint (FP) with respect to different frequency ranges $FP = 1.2 \times H \times (\lambda/d)$ m; where diameter of antennas = 50 cm; λ = C/f m and aircraft speed = 300 km/h, c is the speed of light, f the frequency and λ is the wavelength.

Dwell time can be obtained for various altitudes with respect to different frequencies; footprint (FP) and dwell time are given in Table 4.

$$\text{Dwell time} = \frac{\text{Time taken to move one footprint}}{\text{Total number of footprints}}.$$

Tables 5 and 6 show the relationship between sensitivity and integration time for different noise factor (NF) variations.

Case (i): NF = 1 dB (F = 1.26), T_A = 300 K; T_N = 78 K (F = 1.26), B is bandwidth and τ is integration time.

Case (ii): NF = 2 dB (F = 1.6), T_A = 300 K; T_N = 180 K (F = 1.6); B is bandwidth and τ is integration time.

$$\text{Sensitivity} = \Delta T = \frac{T_A + T_N}{\sqrt{B\tau}} \text{ Kelvin}.$$

Table 7 shows swath width based on altitude and the respective scan angle. Swath width = $2H$; where H is the altitude (for 45° scan angle). Table 8 shows variation of integration time with respect to bandwidth and ΔT.

Figure 4 shows the variation of NF with respect to temperature. Minimum temperature measured = T_1 = 3 K; maximum temperature measured = T_2 = 320 K, where B = 200 MHz; Boltzmann constant, $K = 1.38 \times 10^{-23}$ J/K. The input power signal levels are $P_1 = KT_1$, B = 0.0082 pW and $P_2 = KT_2$, B = 0.883 pW.

Table 3. Footprint (m) for various antenna sizes and altitudes

Altitude (H, km)	Antenna size (d; cm)				
	20	30	40	50	60
1	FP: 19.8	FP: 13.2	FP: 9.9	FP: 7.92	FP: 6.6
2	FP: 39.6	FP: 26.4	FP: 19.8	FP: 15.84	FP: 13.2
3	FP: 59.4	FP: 39.6	FP: 29.7	FP: 23.76	FP: 19.8
4	FP: 79.2	FP: 52.8	FP: 39.6	FP: 31.68	FP: 26.4
5	FP: 99.0	FP: 66.0	FP: 49.5	FP: 39.60	FP: 33.0
6	FP: 118.8	FP: 79.2	FP: 59.4	FP: 47.52	FP: 39.6
7	FP: 138.6	FP: 92.4	FP: 69.3	FP: 55.44	FP: 46.2
8	FP: 158.4	FP: 105.6	FP: 79.2	FP: 63.36	FP: 52.8

Table 4. Variation of FP (m) and dwell time (ms)

	f = 5.3 GHz, λ = 0.0566 m		f = 6.0 GHz, λ = 0.05 m		f = 6.9 GHz, λ = 0.0434 m		f = 11 GHz, λ = 0.0272 m	
Altitude (H, km)	FP (m)	Dwell time (ms)	FP (m)	Dwell time (ms)	FP (m)	Dwell time (ms)	FP (m)	Dwell time (ms)
2	271.68	68	240	56	208.70	42	130.9	16
4	543.36	135	480	112	417.40	85	261.79	33
6	815.04	217	720	168	626.11	127	392.73	50
8	1086.72	290	960	224	834.82	170	523.64	67

Table 5. Variation of sensitivity and integration time (τ, ms) for NF = 1 dB

τ	ΔT (K) at B = 100 MHz	ΔT (K) at B = 150 MHz	ΔT (K) at B = 200 MHz
10	0.378	0.308	0.267
20	0.267	0.218	0.189
40	0.189	0.154	0.134
60	0.154	0.126	0.109
80	0.134	0.109	0.094
100	0.119	0.097	0.084
500	0.053	0.043	0.037
1000	0.037	0.030	0.026

Table 6. Variation of sensitivity and integration time (τ, ms) for NF = 2 dB

τ	ΔT (K) at B = 100 MHz	ΔT (K) at B = 150 MHz	ΔT (K) at B = 200 MHz
10	0.48	0.392	0.34
20	0.34	0.277	0.24
40	0.24	0.196	0.17
60	0.196	0.16	0.138
80	0.17	0.138	0.12
100	0.152	0.124	0.107
500	0.068	0.055	0.048
1000	0.048	0.04	0.034

Table 7. Swath width and altitude variation

Altitude (H, km)	2	4	6	8
±45° Conical scan swath (km)	4	8	12	16

Conclusion

The satellite will be optimized to carry V and H polarization channels for microwave radiometer. If spacecraft resources permit, the 90 GHz radiometer will be complemented with 183 GHz humidity sounder with a shared local oscillator source at 90 GHz (91.5 GHz – multiplied to act as local oscillator for 183 GHz). On-board recorder will be used to record data from inaccessible regions. We will configure SAR in radiometer receiver mode to measure

Table 8. Variation of bandwidth with respect to integration time (τ, ms)

τ	ΔT (K) at B = 500 MHz	ΔT (K) at B = 1000 MHz	ΔT (K) at B = 1.5 GHz	ΔT (K) at B = 2 GHz
10	1.073	0.759	0.619	0.536
20	0.759	0.536	0.438	0.380
30	0.619	0.438	0.357	0.309
40	0.536	0.379	0.309	0.268
50	0.480	0.339	0.277	0.240

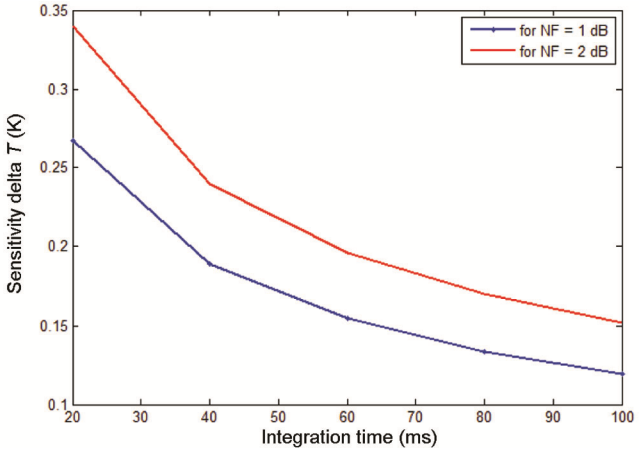

Figure 4. Typical radiometric sensitivity ΔT (K) versus integration time (ms) for BW = 100 MHz in C/X band.

SST and gross soil moisture over vast expanses of agricultural lands, especially in Punjab and Haryana.

Scientific features in support of payloads are as follows: (1) Emissivity of snow/ice is more than 0.9, while that of water is 0.4; thus a very large contrast in brightness temperature signature (260 K against 140 K) can be detected. (2) With the dielectric constant of 3.1 for snow/ice, compared to 81 for water, electromagnetic signals from the radar can penetrate several hundred metres even in the L-band (1–2 GHz).

1. Kent, E. C. and Kaplan, A., Toward estimating climatic trends in SST. Part III: systematic biases. *Proc. J. Atmos. Ocean. Technol.*, 2006, **23**(3), 487–500.
2. Gloersen, P. and Barath, F. T., A scanning multichannel microwave radiometer for nimbus-G and SeaSat-A. *Proc. IEEE J. Oceanic Eng.*, 1977, **2**, 172–178.
3. Ulaby, F., Moore, R. K. and Fung, A. K., *Microwave Remote Sensing: Active and Passive, vol. I: Microwave Remote Sensing Fundamentals and Radiometry*, Addison-Wesley Publishing Company, United States, 1981.
4. Ulaby, F., Moore, R. K. and Fung, A. K., *Microwave Remote Sensing: Active and Passive, vol. II. Radar Remote Sensing and Surface Scattering and Emission Theory*, Addison-Wesley Publishing Company, United States, 1982.
5. Jilani, R., Haq, M. and Naseer, A., A study of glaciers in North Pakistan. Pakistan Space and Upper Atmosphere Research Commission (SUPRCO), 2010.
6. Singh, K. K., Mishra, V. D., Singh, D. K. and Ganju, A., Estimation of snow surface temperature for NW Himalayan regions using passive microwave satellite data. *Indian J. Radio Space Phys.*, 2013, **42**, 27–33.
7. Bajracharya, S. R., Mool, P. K. and Shrestha, B. R., *Global Climate Change and Melting of Himalayan Glaciers*, ICFAI University Press, India, 2008, pp. 28–46.
8. Negi, H. S., Thakur, N. K., Ganju, A. and Snehmani, Monitoring of Gangotri glacier using remote sensing and ground observations. *J. Earth Syst. Sci.*, 2012, **121**(4), 855–866.
9. Wager, A. C., Mapping the depth of a valley glacier by radio ECHO Sounding. *Br. Antarct. Surv., Bull.*, 1982, **51**, 112–123.
10. http://www.himalaya2000.com/himalayan-facts/himalayanglaciers.html
11. http://www.npr.org/2012/04/24/151206843/melt-or-grow-fate-of-himalayan-glaciers-unknown
12. http://en.wikipedia.org/wiki/Re-treat of glaciers_since_1850
13. Williams Jr, R. S. and Ferrigno, J. G., Satellite image atlas of glaciers of the world – glaciers of India. *Proc. US Geol. Surv. Prof. Pap.*, F159-F191, 2010.
14. Skou, N., *Microwave Radiometer Systems: Design and Analysis*, Artech House, 1981.
15. Williams Jr, R. S. and Ferrigno, J. G., Satellite image atlas of glaciers of the world – glaciers of Pakistan. *Proc. US Geol. Surv. Prof. Pap.*, 1386, 2010, 349.
16. Williams Jr, R. S. and Ferrigno, J. G., Satellite image atlas of glaciers of the world – glaciers of Afghanistan. *Proc. US Geol. Surv. Prof., Pap.*, 1386–F-2, F-167-F-199, 2010.
17. Williams Jr, R. S. and Ferrigno, J. G., Satellite image atlas of glaciers of the world – glaciers of Bhutan. *Proc. US Geol. Surv. Prof., Pap.*, 1386–F-2, F-321-F-334, 2010.
18. Thangadurai, N. and Vasudha, M. P., A review of antenna design and development for Indian Regional Navigational Satellite System. In Proceedings of IEEE International Conference on Advanced Communication Control and Computing Technologies, Ramanathapuram, 2016, pp. 299–306.
19. Williams, Jr. R. S. and Ferrigno, J. G., Satellite image atlas of glaciers of the world – glaciers of China. *Proc. US Geol. Surv. Prof., Pap.*, 1386–F-2, F-127-F-166, 2010.
20. Xu, J., Grumbine, R. E., Shrestha, A., Eriksson, M., Yang, X., Wang, Y. and Wilkes, A., The melting Himalayas: cascading effects of climate change on water, biodiversity and livelihoods. *Conserv. Biol.*, 2009, **23**(3), 520–530.
21. Gloersen, P. and Hardis, L., The scanning multichannel microwave radiometer (SMMR) experiment. In *Nimbus 7 Users Guide* (ed. Madrid, C. R.), National Aeronautics and Space Administration Goddard Space Flight Center, Maryland, USA, 1978.

Received 2 March 2017; revised accepted 11 February 2019

doi: 10.18520/cs/v116/i10/1715-1720